The Electrochemical Society
Advancing solid state & electrochemical science & technology

Capacity Recovery Effect in Commercial LiFePO4 / Graphite Cells

Capacity Recovery Effect in Commercial LiFePO4 / Graphite Cells

Franz B. Spingler,[1,z] ![ORCID] **Maik Naumann,**[1,z] ![ORCID] **and Andreas Jossen**[1,2,z] ![ORCID]

[1]*Institute of Electrical Energy Storage Technology, Technical University of Munich (TUM), 80333 Munich, Germany*
[2]*Munich School of Engineering (MSE), Technical University of Munich (TUM), 85748 Garching, Germany*

We report a significant capacity recovery effect of more than 10% after continuous shallow cycling of commercial LiFePO4/ Graphite cells. In a previous study on a LiFePO4/Graphite cell, we observed that capacity losses were more severe with shallow cycles than with full cycles. Herein, the effects of shallow cycling on aging are investigated in detail using three different LiFePO4/ Graphite cell models, two 26650-type and one 18650-type. It is shown that a large portion of the capacity losses that occur with shallow cycling can be recovered by holding the cells at 0% or 100% state of charge. Differential voltage analysis and post-mortem experiments suggest that these capacity losses are caused by strongly non-uniform lithium distributions in the electrodes. Hypothetical mechanisms are presented and discussed that could lead to such non-uniform distributions of lithium.

The existence of a steady, irreversible loss of the usable capacity of lithium-ion batteries as a function of time, charge throughput and other operating parameters is an established fact among researchers and users of battery technology. Reversible losses, however, are rarely observed. In Refs. 1–3, large "anode overhang" areas, which refers to areas of active material that do not face a cathode counterpart, have been identified as a cause of reversible losses of the usable capacity. Depending on the usage profile of the cell, lithium-ions may diffuse into these overhang areas and, in consequence, be inaccessible in the short term. In this paper, we investigate a different, but related, phenomenon, where continued shallow cycling around medium states of charge (SOCs) leads to non-uniform lithium distribution in the electrodes of a commercial LiFePO4/Graphite (LFP/C) cell, which results in a reversible loss of capacity. The observed capacity losses of up to 20% are too great to be caused by the cell's overhang areas. Smaller reversible losses of capacity of up to 1.5% in NiMnCoO2/Graphite cells have been associated with non-uniform lithium distribution.[4]

The phenomenon of reversible capacity losses with shallow cycles was first observed in the course of a 29-month aging study.[5,6] Herein, we present a thorough experimental study of this phenomenon using three different cylindrical cells with a LFP/C chemistry. First, the capacity loss is quantified as a function of various cycle depths and mean states of charge (SOCs). Second, recovery strategies are tested and discussed with the help of differential voltage analysis (DVA). Third, the assumption of uneven lithium distribution in the electrodes is underpinned with post-mortem findings and lastly, hypotheses are presented that could explain the formation of such a non-uniform lithium distribution during cycling.

The main part of this paper is divided into an experimental section, a mostly descriptive results section and a discussion of the results.

Experimental

Commercial cylindrical cells.—Widely available Sony/Murata US26650FTC1 LFP/C cells were used in the main experiments. The rated capacity of these cells is 2.85 Ah at 0.1 C and 25 °C, however, here and in previous studies,[6,7] we have consistently obtained around 3.0 Ah. Further technical data is presented in Table I. The jelly roll design is shown in Fig. 1. In the outermost winding of the jelly roll, the anode sheet is single-side coated, resulting in a relatively small *overhang area*, where the anode has no cathode counterpart. In experiments that were conducted to test whether the effects we

observed with the Sony cells also appear in other LFP/C cells, 2.3 Ah ANR26650M1B and 1.1 Ah APR18650M1A cells from A123 were used.

Cycle aging procedure.—All cycling except capacity check-ups was done at 1 C charge/1 C discharge. Cut-off voltages were 2.0 V and 3.6 V, respectively. In full cycles, a constant voltage (CV) phase until C/20 on discharge and until C/30 on charge was included, as indicated in the cell data sheet. In a previous study,[8] we found accelerated aging in cells that experienced repeated shallow cycles around medium SOCs. In this study, in order to investigate this phenomenon thoroughly, cells were cycled around different mean SOCs ranging from 25% to 75% and with various symmetrical charge-throughputs per charge/discharge ranging from 5% to 100% of the cell capacity. Table II provides an overview of the cycling conditions.

Temperature during cycling.—The initial set of experiments, covering 11000 FEC (full equivalent cycles) of the Sony cell, was conducted at 40 °C, corresponding to the experimental design of our previous study.[8] After it was determined that the reversible capacity loss was similar at a temperature of 25 °C, the second set of experiments was done at 25 °C.

Charge/discharge rates.—Charge and discharge rates during cycle aging were mostly 1 C. A limited number of experiments were conducted at 0.5 C and 2 C to investigate the effect of the charge/discharge rate on the capacity loss with shallow cycles.

Capacity check-ups.—Capacity was measured by a 0.1 C discharge with a C/20 CV phase following a 0.5 C charge with a C/30 CV phase in 100-FEC-intervals.

Recuperation of usable capacity.—Preliminary tests had shown that the application of several full cycles as well as storage at 100% SOC or 0% SOC could help restore a large part of the capacity lost due to shallow cycles. It is hypothesized that the main cause of the loss of useable capacity is a lateral reallocation of lithium-ions in the electrodes. A potential gradient across the electrodes would be a driving force to re-homogenize the electrodes. A significant potential gradient due to non-uniform lithium distribution is most likely to occur at SOCs where the cells' equilibrium voltage characteristic has a large gradient, too. In an LFP/C cell, the voltage characteristic is very steep both at 0% SOC and at 100% SOC, as both materials exhibit a steep increase in potential when they are almost completely delithiated. In consequence, the effects of holding the cell both at 0% SOC and 100% SOC for an extended period of time were investigated in detail. Cells that had previously been cycled for

[z]E-mail: franz.spingler@tum.de; maik.naumann@tum.de; andreas.jossen@tum.de

Table I. Characteristics of Sony US26650FTC1 cylindrical cells.

Cell type and chemistry	Cylindrical 26650, Lithium-Iron-Phosphate/Graphite
Anode sheet size (L × W × H)	1590 mm × 57 mm × 131 μm
Cathode sheet size (L × W × H)	1485 mm × 56 mm × 161 μm
Current collector thickness	Anode: $\sim$11 μm/Cathode: $\sim$13 μm
Coating thickness	Anode: 60 μm/Cathode: $\sim$74 μm
Max. cont. charge/discharge rate	1 C/6 C
Upper and lower cut-off volt.	3.6 V/2.0 V

600 FEC with 20% cycle depth around 50% SOC and had reached approx. 83% relative capacity were used for the recuperation study. They were held at 0% or 100% SOC for 7 d by keeping their voltage constant ("voltage hold") at 2.0 V and 3.6 V respectively, and were then subjected to a capacity check-up. This procedure was repeated five times, resulting in a total of 35 d of recovery. Generally, chamber temperature was 25 °C. Two cells, however, were tested at 45 °C and 0% SOC, to find out whether the recovery process was temperature dependent. Another two cells were alternated between 0% SOC and 100% SOC in four 42 h intervals with an initial charge/discharge time of approx. 1 h and subsequent maintenance of the charge level until the end of the interval. This meant that they underwent 7 d of recuperation in between each capacity check-up.

dV/dQ analysis.—Discharge data from the 0.1 C capacity check-ups were used for dV/dQ analysis. Cells were cycled to 600 FEC and thereafter underwent recuperation at 0% SOC (voltage hold 2.0 V) over 3 d intervals interrupted by capacity check-ups.

Cell opening and post-mortem inspection.—Cells were opened in an argon filled glovebox with oxygen and water levels below 0.1 ppm. 24 h prior to opening, the cells were charged to 50% SOC at a 0.1 C rate. The jelly rolls were disassembled while still wet and then left to dry in the glovebox for approx. one hour. Photographs were taken of the electrodes in front of a gray background paper.

Local SOC measurement via CR2032 half cells.—The aim of the coin cell measurements was to assess the local SOC in each
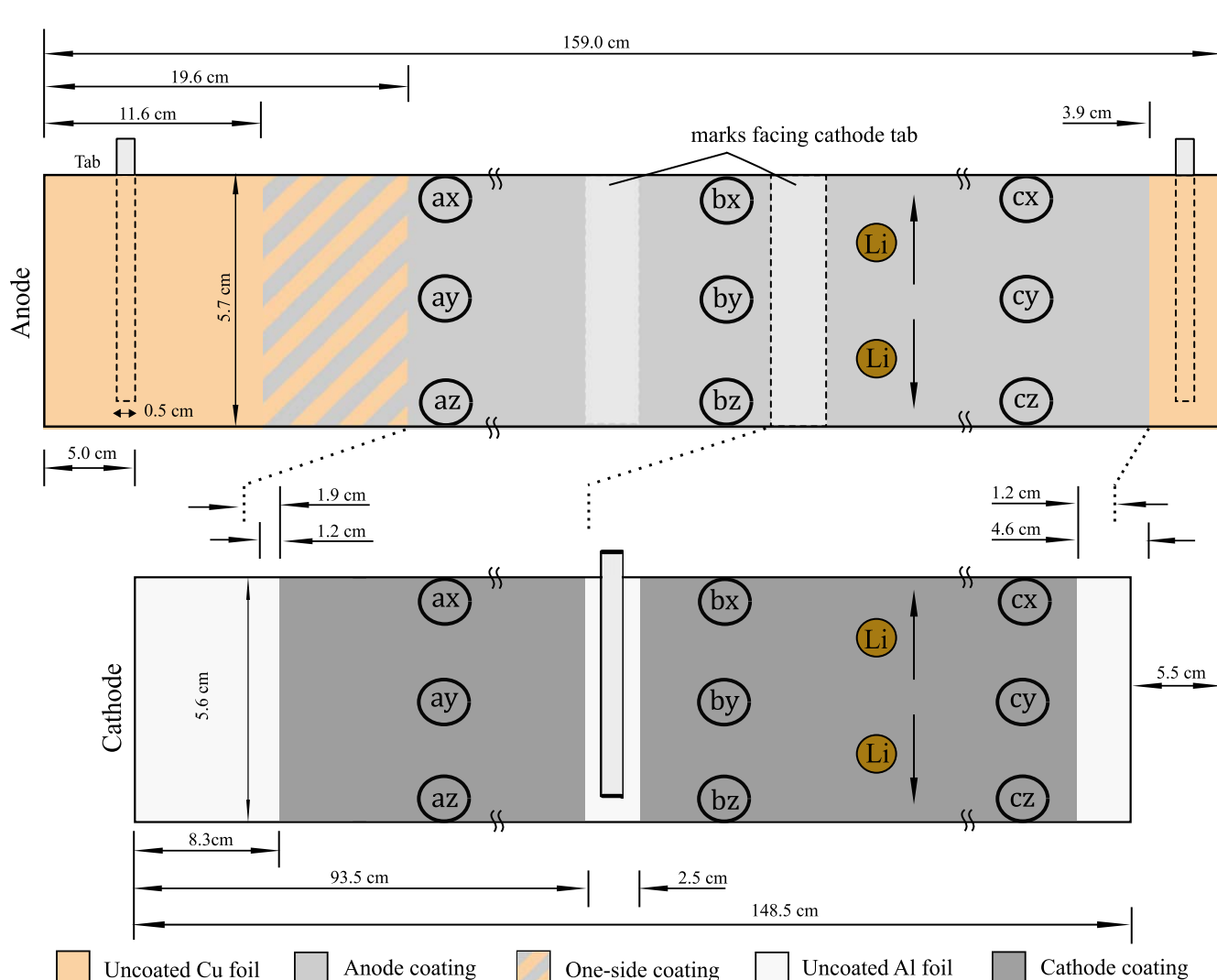

Figure 1. Schematic of the SONY US26650FTC1 jelly roll and electrodes. The graphite anode has one tab on each end, the cathode has a single tab in the center. The nine locations from where coin electrodes were punched out are shown. The "x" and "z" coins were punched out as closely as possible to the edges.

electrode (via the initial discharge) as well as their area-specific reversible capacities. Using a precision punch, 10 mm coins were obtained from nine locations across the electrodes, as shown in the schematic in Fig. 1. Three coins were punched out next to each other at each location. The coin electrodes were dried in the glovebox for at least 24 h. CR2032-type coin cells were assembled using two layers of 16.0 mm diameter VWR 691 glass fiber (260 μm each) as the separator, a 15.6 mm diameter lithium chip (250 μm) as the counter electrode and 1.0 mm plus 0.5 mm spacers. 80 μl of LP57 (3:7 wt EC:EMC 1 Mol LiPF6) were used as the electrolyte. After assembly, the cells were rested for 6 h and then cycled at 0.1 C using a constant current/constant current protocol (CC/CC). The cells made from the graphite anodes were cycled between 10 mV and 1.5 V, beginning with a delithiation of the graphite until the cell reached 1.5 V. The cells made from the LFP cathodes were cycled between 2.0 V and 3.6 V, beginning with a delithiation of the LFP until the cell reached 3.6 V. As the total number of coin cells to be cycled was very large and the number of test channels was limited, cycling was generally stopped after three cycles. However, to test the quality of the cells, some cells were cycled 20 times or for approx. 500 h. No significant capacity fade in the working electrodes was detected.

Results

Loss of usable capacity associated with shallow cycles.—Cells were cycled around various mean SOCs and with different cycle depths as detailed in Table II. Figure 2b illustrates the cycle aging scheme: every 100 FEC, cycling is interrupted by a capacity check-up. Capacity retention vs FEC for over 10,000 FEC is shown in Figs. 2a and 2c. Figure 2a shows the results of varying cycle depth while keeping the mean SOC constant at 50%. Figure 2c shows the results of varying the mean SOC while keeping the cycle depth constant at 20%. In both graphs, the capacity retention with full cycles (0% SOC–100% SOC) is shown for reference. In cells subject

Table II. Overview of mean SOCs and cycle depths investigated in this study.

Mean SOC/%	Cycle depth/%
25	20
40	10, 20
45	10
50	5, 10, 20, 40, 60, 80, 100
55	10
60	10, 20
65	10
70	10
75	10, 20

to full cycles, capacity loss is almost linear after slightly higher losses in the first 300 cycles. 80% relative capacity is reached only after approx. 6500 full cycles. When the cycle depth is reduced to 80%, the initial rate of capacity loss is slightly higher until 2000 FEC and is slightly lower thereafter. For further reduced cycle depths, which maintain a charge/discharge symmetry around 50% SOC, initial capacity loss is more drastic. With cycle depths between 5% and 40%, the loss of usable capacity is between 13% and 21% after 1000 FEC, compared to only 6% with full cycles. The most severe capacity loss occurs with 20% (40% SOC–60% SOC) and 10% (45% SOC–55% SOC) cycle depth. These results are in agreement with Ref. 8, where, for a LFP/C cell, capacity loss with cycle depths from 10% to 60% was found to be higher than with full cycles during 2000 FEC. The capacity retention vs FEC curves of both reach a minimum at approx. 1500 FEC, after which the capacity recuperates slightly and levels off between 4000 and 7000 FEC and then decreases slightly again, at a slower rate than with full cycles. Cycling between 30% SOC and 70% SOC leads to a similarly fast
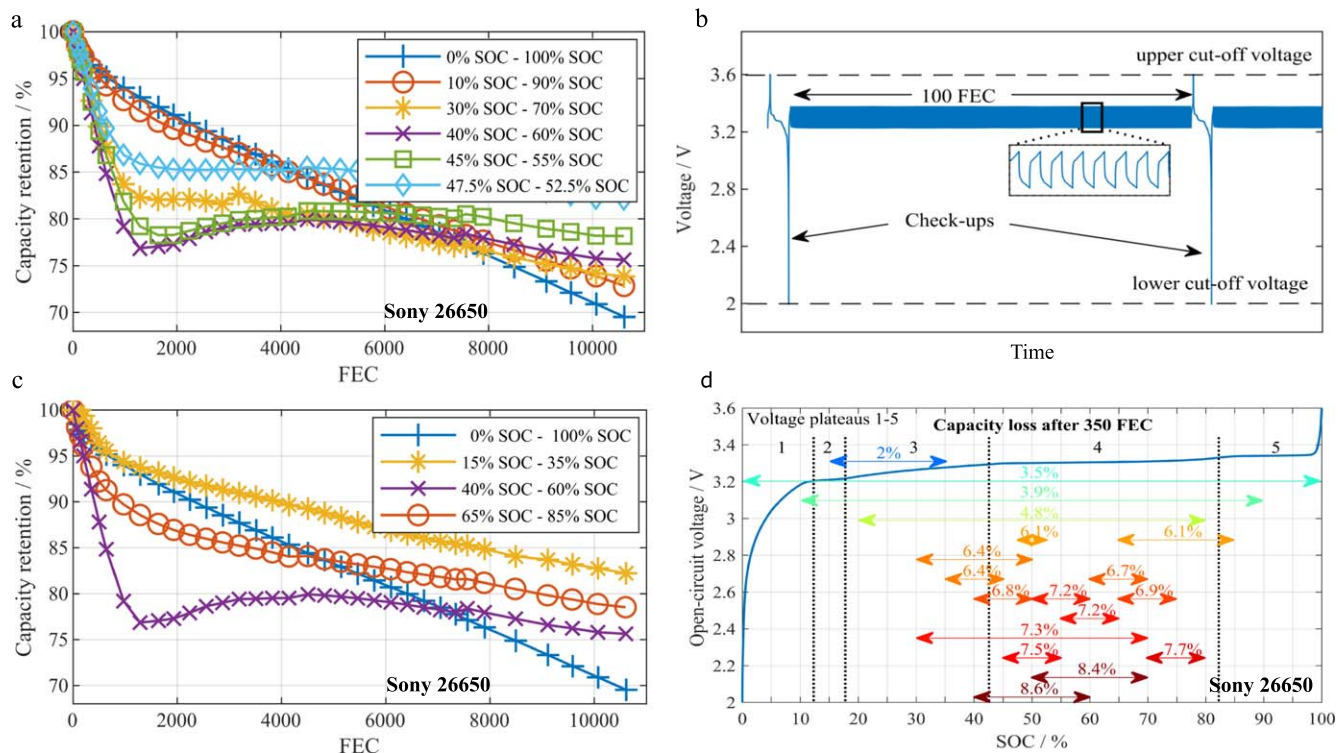

Figure 2. (a) Capacity retention vs FECs as a function of cycle depth and mean SOC (c). Capacity retention with full cycles is shown in blue in both graphs for reference. Cycling with low cycle depths around 50% SOC leads to much faster capacity losses than full cycles. (b) Cycling procedure exemplarily shown for 40% − 60% SOC. (d): Capacity losses in % after 350 FEC as a function of cycle depth and mean SOC. The equilibrium voltage curve of the cell with its characteristic plateaus is displayed for reference. In SOC windows without significant gradients in the equilibrium voltage curve, capacity losses are relatively small.
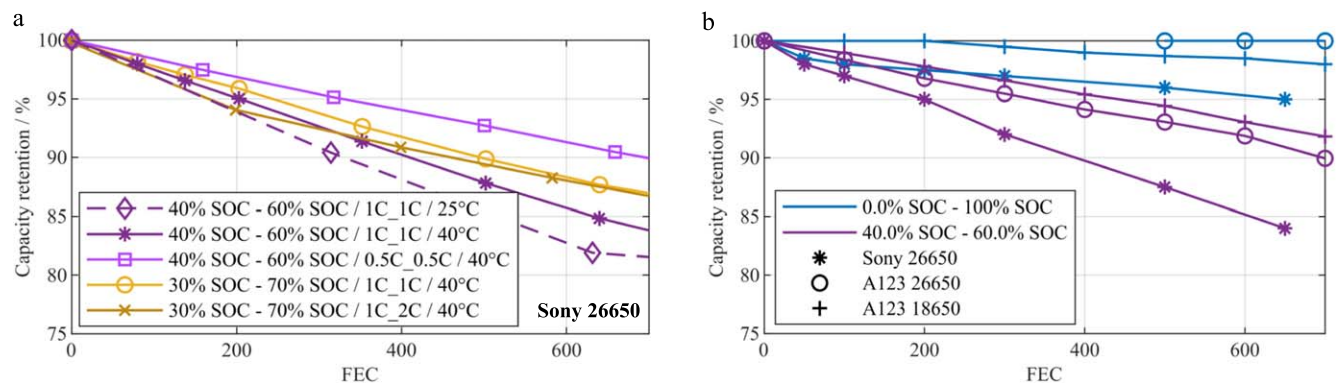
Figure 3. (a) Variation of temperature and C-rate. At a current of 0.5 C, the cells lose less capacity than at 1.0 C. Reducing the temperature to 25 °C increases the capacity losses as compared to 40 °C. (b) Comparison of the Sony cell with two LFP/C cells from manufacturer A123 (all at 25 °C). While the A123 cells generally have a higher capacity retention, all of these cells lose significantly more capacity with shallow cycles than with full cycles. A123 18650 full cycle data is adopted from Ref. 9.

capacity decrease, which levels off shortly after 1500 FEC and continues after 4000 FEC. Beyond 7000 FEC, capacity retention with shallow cycles is higher than with full cycles. Finally, at 10,000 FEC, the amount of capacity lost is a function of cycle depth with higher cycle depth corresponding to higher capacity loss. The best capacity retention at 10,000 FEC is obtained by cycling between 47.5% SOC and 52.5% SOC: After an initial decay to 86% relative capacity at 1500 FEC, capacity remains almost constant.

Figure 2c shows that the rate of capacity loss is just as dependent on mean SOC as it is on cycle depth: The capacity decay when cycling between 65% SOC and 85% SOC is much slower than with cycling between 40% SOC and 60% SOC. However, in the first 1000 FEC, capacity still decays quicker than with full cycles. Only cycling at lower mean SOCs, i.e. between 15% SOC and 35% SOC, leads to a slower capacity decay than full cycles in this FEC interval. The combination of the results shown in Figs. 2a and 2c suggests that the SOC window is the relevant parameter, rather than cycle depth or mean SOC alone. This idea is reflected in the experiments presented in Fig. 2d, which shows the capacity losses after 350 FEC associated with all of the cycle depth and mean SOC combinations tested. The highest losses, over 8%, occur between 40% SOC and 60% SOC and between 50% SOC and 70% SOC. Several other SOC windows between 30% SOC and 80% SOC lead to considerable losses over 6%. When the SOC window exceeds the voltage plateaus designated "3" and "4", the cycling losses are considerably lower.

Temperature, and C-rate variation, other cells.—Figure 3a shows capacity retention over 700 FEC for different C-rates and temperatures. In addition to testing 1 C charge/1 C discharge, 0.5 C charge/0.5 C discharge and 1 C charge/2 C discharge at a chamber temperature of 40 °C, the 1 C charge/1 C discharge experiment was repeated at 25 °C. The effect of changing the discharge rate from 1 C to 2 C was negligible. At 0.5 C/0.5 C, however, capacity retention was higher than at 1 C/1 C. Temperature seems to have a limited effect on capacity loss, as the cells at 25 °C lost capacity at a slightly higher rate compared to 40 °C.

Figure 3b compares the capacity retention over 700 FEC of the A123 18650 and A123 26650 to the 26650 Sony cell. Chamber temperature was 25 °C throughout and only full cycles and 40% SOC−60% SOC cycles were investigated. The A123 cells exhibit the same behavior as the Sony cell: shallow cycles lead to a much more rapid capacity decay than full cycles. In both cycling scenarios, the A123 has a better overall capacity retention. Considering the fact that their capacity loss during the first 300 full cycles is zero or negative, their better overall capacity retention may be due to some capacity recovery from the overhang areas, which, at least in the case of the A123 18650, is known to be of significant size.[1]

Recuperation of usable capacity.—The recuperation tests were performed on cells that had been cycled between 40% SOC and 60% SOC for 700 FEC and had reached around 83% relative capacity. Two cells that had undergone 700 full cycles and had reached 95% relative capacity were included for reference. The recuperation strategies were i) voltage hold at 2 V/0% SOC ii) voltage hold at 3.6 V/100% SOC and iii) alternating between 2 V and 3.6 V. More details are provided in the experimental section. Figure 4 shows an examplary recuperation process with voltage hold at 2 V. The upper graph shows voltage during check-ups and recuperation and the capacity retention, which increases after every interval. The lower graph shows current and accumulated charge throughput of every recuperation interval. Charge throughput decreases rapidly as the recuperation proceeds. The total charge throughput from all intervals is −690 mAh, while the total change in capacity retention amounts
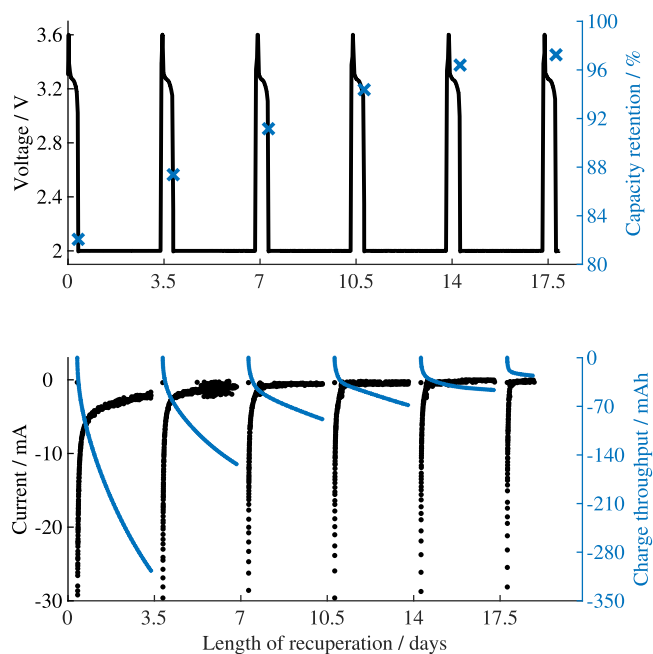

Figure 4. Recuperation procedure for 2 V hold strategy. Upper graph: Voltage during capacity check-ups and recuperation intervals; capacity retention as determined in check-ups. Lower graph: Current and charge throughput during recuperation intervals. The total charge throughput from all intervals is −690 mAh, while the total change in capacity retention amounts to 455 mAh.
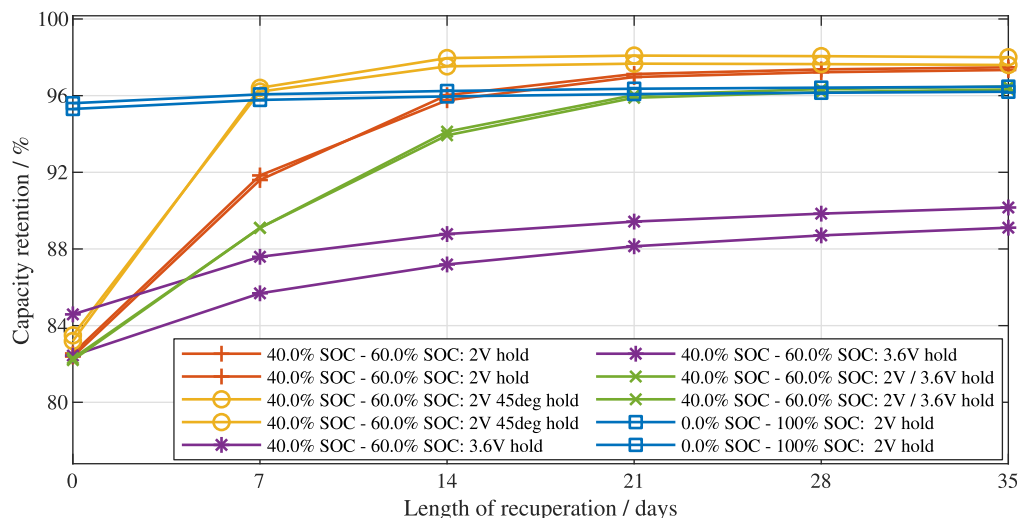
Figure 5. Recuperation of usable capacity as a function of days for various recuperation strategies. Cells held at 2 V or 0% SOC recuperate at the highest rate. Increased temperature further accelerates the recuperation process. After full cycle aging, almost no capacity can be recuperated. If not indicated otherwise, temperature was 25 °C. (Note: insert degree symbol.)

to 455 mAh. These numbers suggest that the "inactive" capacity that is being accessed during recuperation is partly re-actived.

The results of the recuperation tests shown in Fig. 5 show a clear trend: both the rate of capacity recuperation and the final amount of capacity recuperated are highest at 2 V hold, followed by alternating between 2 V/3.6 V hold and 3.6 V hold. Increasing the temperature to 45 °C seems to accelerate the recuperation process. Generally, the rate of recuperation declines rapidly with time. After 35 d of 2 V hold at 25 °C, the relative capacity was 98%, which means that approx. 89% of the lost capacity had been recovered. At this temperature, between 14 and 21 d were needed to reach 97% relative capacity. In contrast, 97% relative capacity was reached after only 7 d at 45 °C. The relative capacity of the cells that had undergone full cycles before the recuperation test, recovered only slightly from 95% to 96.5%.

dV/dQ analysis.—Another set of cells was cycle aged between 40% SOC and 60% SOC for 620 FEC and thereafter underwent the 2 V hold recuperation strategy over 72 h periods, interrupted by capacity check-ups. 72 h periods were implemented instead of 168 h (7 d) uninterrupted, so that capacity recuperation could be tracked more closely. Figure 6 shows the discharge voltage curves of capacity check-ups during aging. After 200 FEC, a voltage plateau is visible at the beginning of discharge and becomes more distinct as the number of FECs increases. Such plateaus typically occur during a lithium stripping process on discharge following lithium plating during charging.[10–15] The amount of stripped lithium is thought to be

equivalent to the length of the plateau[10] which is approx. 0.15 mAh in the discharge curve after 600 FEC. Figure 7 shows the dV/dQ curves obtained from discharge voltage curves of capacity check-ups during aging and recuperation. The first two graphs on the right, b) and d), are details of the graphs a) and c) on the left. The dV/dQ curves run from right (100% SOC) to left (0% SOC) in each graph. In Figs. 7a and 7b, a peak in the curve of the fresh cell is visible when about 2.3 Ah capacity remains, which is thought to demark the end of the LiC_6/LiC_{12} voltage plateau (Upon delithiation, the graphite anode undergoes a structural change from LiC6 to several discrete lower-lithiated phases. The co-existence of phases leads to characteristic voltage plateaus.[16,17]) of the graphite anode. This peak serves as a well-defined anode-SOC marker. The charge throughput between 0% SOC and this marker is denoted Q_1, while Q_2 represents the number of ampere hours between the plateau and 100% SOC, as illustrated by the arrows in Fig. 7f. Both Q_1 and Q_2 decrease with cycling and increase again during recuperation, see Fig. 7e. The values of Q_1 and Q_2 are provided in Table III. A decrease of Q_1 is linked to a decrease of the (accessible) anode capacity. A change of Q_2, which represents the distance between the graphite peak and the fully delithiated state of the cathode, indicates a shift of the electrode balancing due to a loss of (accessible) cycleable lithium.[18,19] Figure 7b shows that the height of the peak at 2.3 Ah decreases with cycling, while the peak width increases. The broadening of this graphite peak has been associated with non-uniform lithium distribution.[20] In Figs. 7a and 7b, another peak appears at around 2.5 Ah remaining capacity after 200 FEC. The peak's height increases dramatically until 620 FEC. The peak results from the voltage plateaus in the discharge curves as shown in Fig. 6, which, as discussed above, may indicate a lithium stripping process.

Non-uniform lithium distributions in both anode and cathode could potentially explain all of these phenomena: The mixed potential of a more delithiated part of the cathode and the rest of the cathode, could be large enough to trigger the upper voltage cut-off that defines 100% SOC. The same mechanism could shift the location and width of the graphite peak. The areas with higher local SOCs would contain the non-accessible cycleable lithium. Those areas with higher local SOCs would then be at a higher risk of lithium plating during the capacity check-up cycles (0.5 C charge/ 0.1 C discharge).

Figures 7c and 5d show the dV/dQ curves of check-ups between recuperation intervals of 72 h. After the first 72 h of keeping the cell at 2 V, the prominent peak at 2.5 Ah disappears. The LiC_6/LiC_{12} peak height increases after every recuperation interval, although it does not reach the original height of the fresh cell. Figure 7f shows
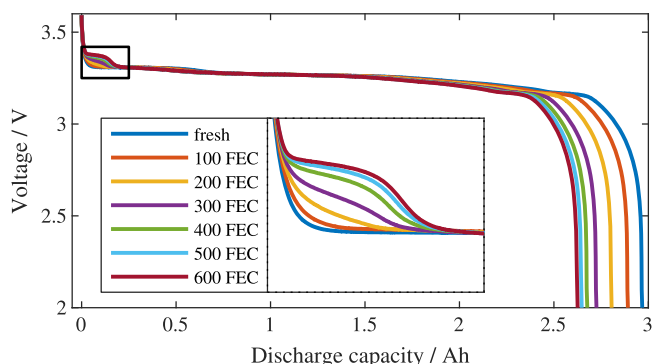

Figure 6. Discharge voltage curves from capacity check-ups during aging. A distinct voltage plateau appears as the number of FECs increases. The voltage plateau may indicate a lithium stripping process.
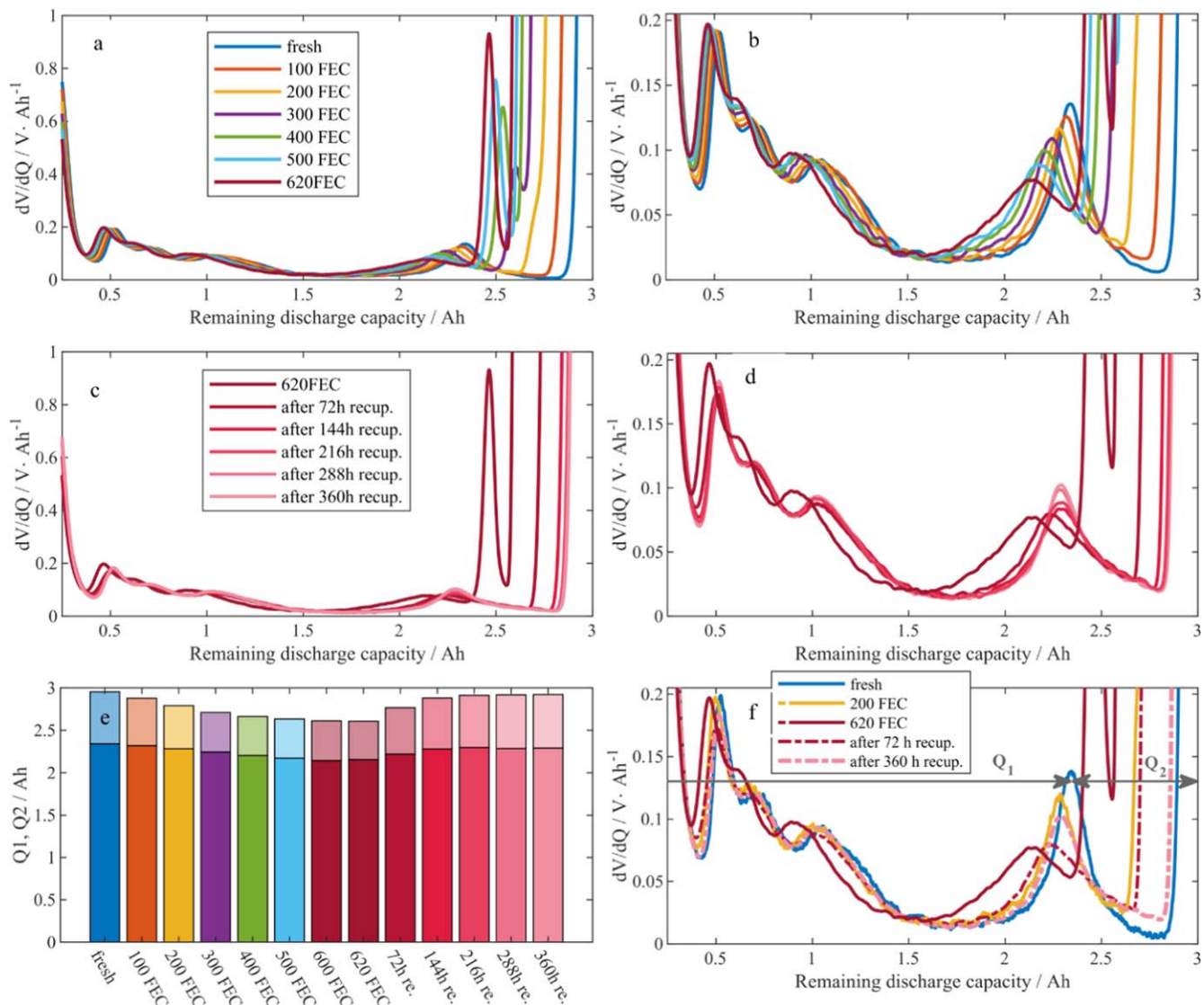
Figure 7. dV/dQ on discharge between 100 FEC-cycling-intervals until 600 FEC (first row) and between 72 h recuperation intervals at 0% SOC (second row). A selection of curves is shown in the third row. Plots on the right are details of the plots on the left. Evolution of usable capacity, Q1 and Q2 during cycle aging and recuperation via 2 V hold. Q1 represents the number of ampere hours between 0% SOC and the LiC6-LiC12 peak, Q2 between the peak and 100% SOC.

selected dV/dQ curves of both aging and recuperation for easier comparison.

Post-mortem analysis.—In order to find evidence for or against non-uniform lithium distribution as suggested by the dV/dQ analysis, a post-mortem analysis was conducted. A total of five cells were opened in the course of this study: Two new/fresh cells, two that had been cycled for 700 FEC between 40% SOC and 60% SOC, and one that had been cycled for 700 FEC with full cycles. In all cells, the overhang areas were clearly visible. Their locations and sizes are shown in the schematic in Fig. 1. The three tabs (two on the anode, one on the cathode) left visible pressure marks on the

electrodes at a distance of up to three windings along the coil. All cycle aged cells had a slightly different-colored stripe in the center of the anodes over their full length. Otherwise, the electrodes of the cell aged with full cycles looked the same as those of the fresh cells. Interestingly, the cells cycled between 40% SOC and 60% SOC displayed a distinctive feature: an approx. 5 mm wide distinctly-colored stripe at the upper and lower edges. As can be seen in the photographs in Fig. 8, the stripe is grey in the outer section (the outermost part of the coil) of the anode, and is gold with a violet edge in the middle and core sections. The stripe was also found to be consistently slightly wider towards the core. It is generally accepted that this gold color coincides with the highest lithiation state of

Table III. Evolution of usable capacity, Q1 and Q2 during cycle aging and recuperation via 2 V hold. Q1 represents the amount of ampere hours between 0% SOC and the LiC6-LiC12 peak, Q2 between the peak and 100% SOC.

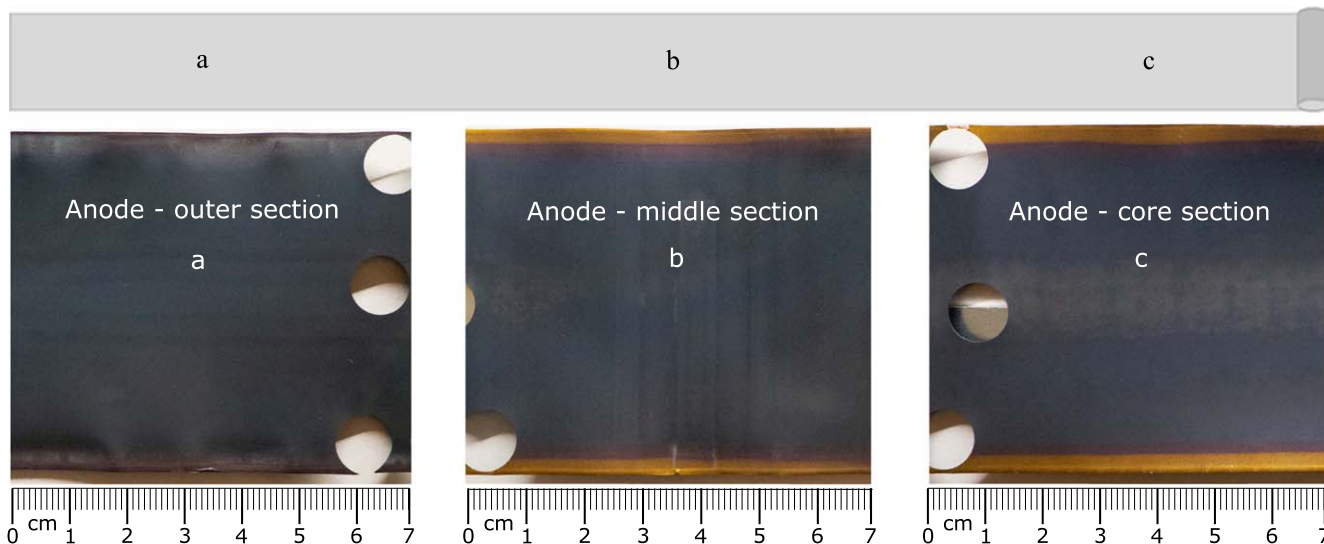|	Fresh	100 cyc.	200 cyc.	300 cyc.	400 cyc	500 cyc	600 cyc	620 cyc	72 h	144 h	216 h	288 h	360 h
Q1/Ah	2.341	2.319	2.283	2.245	2.202	2.170	2.145	2.155	2.220	2.280	2.299	2.285	2.292
Q2/Ah	0.615	0.560	0.509	0.467	0.462	0.464	0.469	0.454	0.548	0.601	0.614	0.634	0.631
Q1 + Q2/Ah	2.96	2.88	2.79	2.71	2.66	2.63	2.61	2.61	2.77	2.88	2.91	2.92	2.92

Figure 8. Post-mortem photographs of the anode after 700 FEC between 40% and 60% SOC. From (a) to (c): Outer, middle, and inner sections of the anode roll with circular holes from punching out the 10 mm electrodes. While the outer section exhibits a grey stripe of approx. 5 mm width along the edges, this band is gold in the middle and inner sections. The cells that were cycled with 700 full cycles had a similar grey stripe in the center but no grey or gold stripe at the edges.

graphite, followed by violet.[17,21–23] This means that the lithiation state at the edges of the anode would have been much higher than in the average cell at 50% SOC. As for the grey stripe in section a of the anode, see Fig. 8, it could be hypothesized that this could be an example of lithium plating, which is associated with grey or silver colored deposits.[24–27] The discharge voltage curve and dV/dQ have already hinted at this possibility. If we assume that on the 5 mm wide stripe across the full length of the electrode, all of the charge between 50% SOC and 100% SOC corresponding to that area were plated during charging in the capacity check-up, the amount of plated lithium would be: $5\ mm/57\ mm\ \times\ 1.5\ Ah = 0.13\ mAh$. This number is close to the approximate amount of charge of 0.15 mAh ascribed to lithium stripping above. The slightly lower temperature in the outer section "a" may have led to stronger lithium plating and a higher degree of irreversibility of the plated lithium relative to the other sections.

Charge distribution.—From anode and cathode, coin electrodes were punched out from the upper and lower edges and in the center ("x", "y", "z") of the outer, middle and core sections ("a","b","c"). The reader is referred to Fig. 1 for reference. These electrodes were assembled in coin cells with a lithium counter electrode and

discharged. The resulting charge distributions in a cycled and in a new cell, both at 50% SOC, are shown in Fig. 9. Each rectangle represents the charge of the respective 10 mm circle. The exact values are provided in Table IV. A quantitative evaluation or the investigation of a charge gradient from edge to the center of the electrode is difficult because the gold-colored stripe at the edge covers only about a third of the 10 mm electrodes that were punched out. Notwithstanding these limitations, Fig. 9 shows that there is clearly more charge, i.e. lithium-ions, at the edges ("x", "z") than in the center ("y") of the anode of the cycled cell. The cathode of the cycled cell has slightly more charge at the edges as well. In the case of the new cell, charge is generally more evenly distributed. While in the new anode no significant charge differences can be observed, the new cathode has slightly more charge in the center compared to the edges. This overall trend is best observed in the lower two graphs of Fig. 9 that show the sum of anode and cathode charge: The cycled cell has a considerably higher cycleable lithium content at the edges, while the new cell has a slightly higher cycleable lithium content in the center. Lithium content also seems to be unevenly distributed along the length of the electrodes. While the middle ("b") and core ("c") sections are quite similar, the outer ("a") section stands out as

Table IV. Areal capacities of coin cells in first discharge. Coin cells were punched out from harvested electrodes at three positions along the electrodes' length ("a", "b", "c") and three positions along the electrodes' height ("x", "y", "z").

Areal capacity of coin cells in first discharge/mAh/cm^2

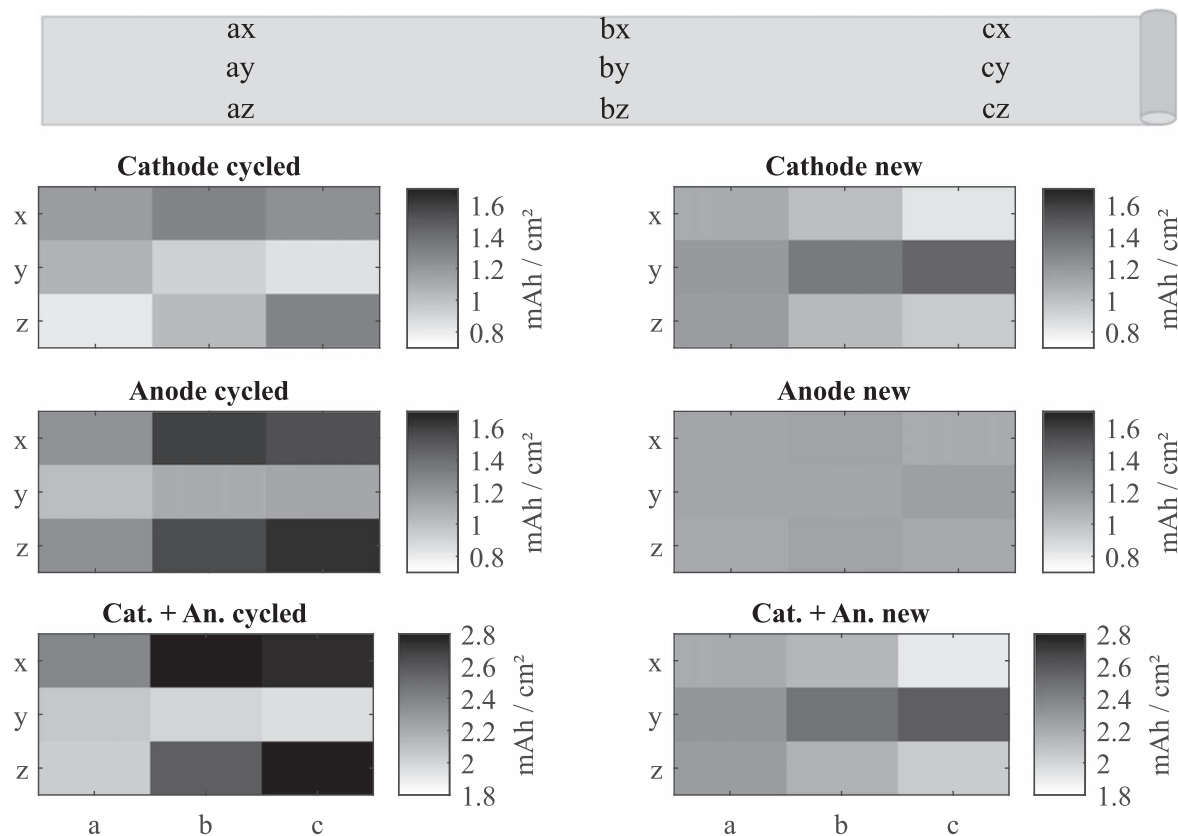|	Cathode cycled			Cathode new		
x	1.16	1.29	1.23	1.08	1.00	0.82
y	1.06	0.92	0.83	1.18	1.34	1.42
z	0.81	1.02	1.29	1.16	1.02	0.94
	Anode cycled			Anode new		
x	1.21	1.58	1.52	1.11	1.13	1.08
y	1.01	1.08	1.11	1.11	1.12	1.15
z	1.22	1.54	1.62	1.10	1.13	1.10
	Cat.+An. cycled			Cat.+An. New		
x	2.37	2.87	2.74	2.19	2.13	1.90
y	2.06	2.00	1.94	2.29	2.46	2.57
z	2.03	2.56	2.92	2.26	2.15	2.04
Loc.	a	b	c	a	b	c

Figure 9. Distribution of charge in the electrodes of cells at 50% SOC. Left column: cell cycled between 40% SOC and 60% SOC for 700 FEC. Right column: fresh cell. Generally, the cycled cell exhibits an accumulation of charge at the edges of both electrodes, while the fresh cell tends to be more homogenous (anode) or has higher area-specific charge in the center than at the edges (cathode).

lithium is more evenly distributed between the edges and the center at this point.

Discussion

The experimental results can be summarized as follows:–Cycling cylindrical LFP/C cells anywhere between 30% SOC and 70% SOC, i.e. where the equilibrium voltage curve's gradient is low, produces significantly higher capacity losses than full cycles.–Keeping the cells at 0% SOC or 100% SOC, i.e. where the equilibrium voltage curve's gradients are high, recovers most of the lost capacity within a couple of days.–Peak broadening observed in the dV/dQ analysis suggests non-uniform lithium distributions in the electrodes–Post-mortem investigations confirm non-uniform lithium distributions in the cells. The areas near the edges had a significantly higher lithium content than the average of both electrodes. This seems likely to be the reason for the loss of usable capacity: The local cell SOC depends on the local SOCs of the anode and cathode. The lower SOC areas would provoke an early "cut-off" on discharge, the higher SOC areas on charge.

Based on the results, it could be hypothesized that the low equilibrium voltage curve's gradient at medium SOCs of LFP/C cells is an insufficient driving force to re-homogenize the SOC within the electrodes should it become non-uniform. Only when the non-uniformity reaches a certain critical point, would the homogenizing forces become more powerful. As a result, the capacity loss levels off after 2000 FEC, cf. Fig. 2b. The hypothesis leads to the question: what causes the SOC to become non-uniform in the first place? Several causes can be envisaged: temperature gradients,[28,29] pressure gradients,[29,30] tab location[31,32] or effects related to non-uniform current density due to defects,[33] covering layers, anode/cathode overlap[34] or overhang areas.[1,3] It could be argued that in the absence of a re-homogenizing driving force, it would be highly

unlikely that local lithium concentrations would remain homogeneous during cell operation. This would only be the case if an improbable combination of perfectly homogeneous electrodes, operating conditions and current density distribution were to occur. From the above mentioned, however, defects are unlikely to have played an important role in the investigated Sony cell. The same is true for overhang areas at the beginning or the end of the electrode spiral. This is the case because firstly, their area is negligible compared to the total electrode area in the case of the Sony cell (see Fig. 1) and secondly, because they could not explain the inhomogeneity in perpendicular direction to the length of the spiral.

Temperature gradients.—During operation, heat is generated quite uniformly across the electrodes. In a cylindrical cell, heat can be exchanged with the environment via the lateral surface as well as the top and bottom surfaces. This leads to temperature gradients in both parallel and perpendicular direction to the cylinder surface.[28,29] Temperature gradients could cause two effects: first, via temperature-dependent electrode kinetics and transport, they lead to gradients in current density, which in turn may lead to a non-uniform SOC. Second, in conjunction with non-zero entropic coefficients, a difference in temperatures results in different equilibrium potentials of the electrodes. The entropic coefficient of graphite varies between -0.2 mV K^{-1} and 0.2 mV/K[35,36] and that of LFP between -0.1 mV K^{-1} and 0.1 mV/K.[35,37] The full cell entropic coefficient is positive over a wide range of medium SOCs,[37] as the entropic coefficient of graphite is positive and is larger in absolute values than the negative LFP coefficient.

If the potential in each electrode is assumed to be uniform, the local SOCs would need to diverge according to the cell or electrode equilibrium potential curve to adjust for the entropic voltage change. This could potentially affect the local cell SOC as well as the local
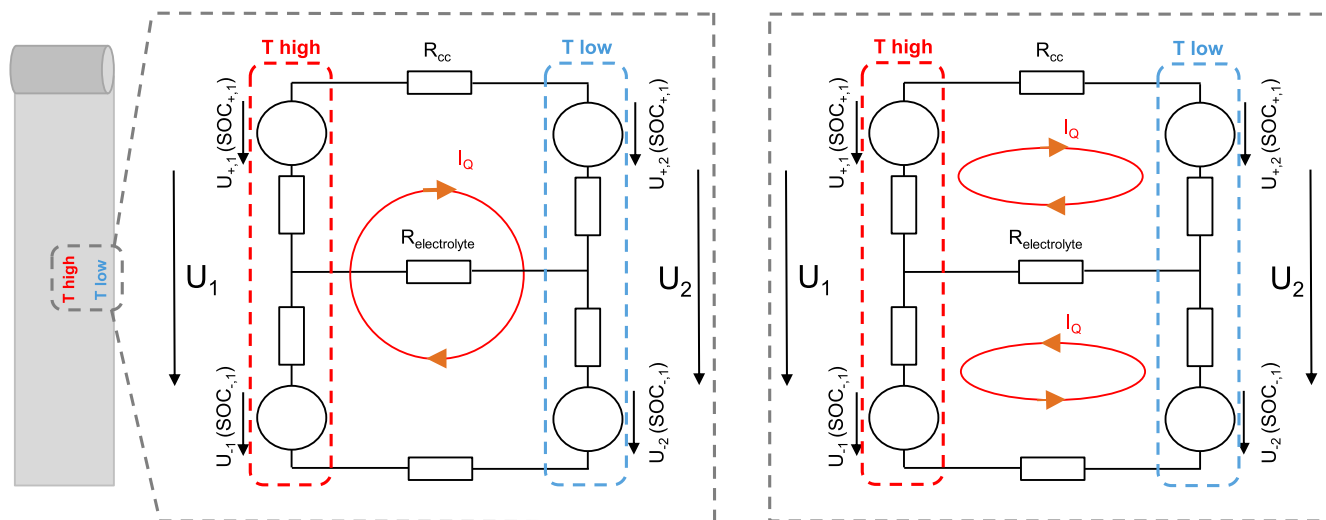
Figure 10. Two mechanisms of temperature-driven charge reallocation based on a simple cell model. Each cell consists of two unit cells connected in parallel via a current collector resistance and an electrolyte resistance. Each unit cell consists of two "electrodes" represented by a voltage source (circles) and a resistance (rectangles). In both schematics, the left unit cell has a higher temperature than the right unit cell. In the left schematic, through-plane currents alter the local cell SOC. In the right schematic, in-plane currents alter the local electrode SOCs.

electrode SOCs. In Fig. 10, two hypothetical mechanisms based on a simple cell model are sketched out. Each model cell consists of two elementary cells at different temperatures (high and low) which are connected in parallel via the current collectors and an ionic path through the electrolyte. Their voltages, U1 and U2, are virtually identical due to the parallel connection via the current collectors. In both model cells, no external current flows into or out of the cell. In the left model cell, through-plane currents alter the local cell SOC. This is an instantaneous reaction to any temperature gradient within a cell, provided the full cell entropic coefficient is non-zero. In the right model cell, in-plane currents alter the local electrode SOCs. As these currents must take the ionic path through the electrolyte, they should be much smaller than the through-plane currents. Nevertheless, they would slowly redistribute the lithium content within each electrode until a new equilibrium dictated by the electrode's entropic coefficient, local equilibrium potential and temperature was reached. In a real cell, both mechanisms should occur simultaneously and influence one another. Could these mechanisms explain the non-uniform lithium distribution we have observed? In a spirally wound cell, due to the good heat conduction of the current collector foils, temperature gradients along the height of the cell are small.[38] However, the equilibrium potential curve of LFP is essentially flat, which means that SOCs could differ considerably even with a temperature difference of a few Kelvin and an entropic coefficient of $-0.1\,\mathrm{mV\,K^{-1}}$. Admittedly, if we assume that the temperature at the electrode edge is slightly lower than in the center, the negative entropic coefficient would result in a lower local SOC at the edge compared to the center, opposite to what is actually observed.

Anode/cathode overlap.—Another possible factor in creating SOC non-uniformity could be geometrical. At the electrode edges, the anode surface projects beyond that of the cathode. This overlap is designed with the aim of avoiding lithium plating on the anode surface. The additional anode surface in the overlap absorbs the locally higher current densities that result from the exposed side faces of the electrodes.[34] Assuming current density and, in consequence, cycle depth are higher at the edges than in the rest of the electrode, two mechanisms that redistribute the lithium content in the electrodes can be conceived:

First, in the back and forth motion of ions between the electrodes, we may think of the location of arrival of an individual ion on the intercalating electrode as following a probability density function: The ion is most likely to take the shortest path, perpendicular to the

electrode surface, and to arrive just opposite from where it de-intercalated. It is less likely to move at a more acute angle to the electrode surface and take a longer path. In an ideal cell this would not lead to non-uniform SOCs as on average, the lateral movements would balance themselves out. However, if there is a "disturbance," this balance may be lost. The edge region, where we assume current densities are higher than elsewhere, could attract more lithium ions than average. Upon repeated cycling, lithium ions would become concentrated at the edges. In electrodes that have significant gradients in their equilibrium potential curves increasing local potentials would counteract these high local current densities, but this would not be the case with LFP.

Second, a "pumping mechanism": If cycle depth is higher at the edges, there will be an in-plane movement of ions to equalize the local SOCs within the electrodes. If this equalization process is much slower in one electrode than in the other (it could be slow in LFP due to its flat voltage characteristic), lithium ions would slowly accumulate at the edge of that electrode. The other electrode's lithium distribution would be uniform. This also disagrees with the experimental evidence. There would need to be some directional process to explain charge accumulation in both electrodes by this pumping mechanism. A possible candidate for this could be asymmetric overpotential in charge/discharge due to hysteresis in the equilibrium potential curves of LFP.[39]

Passivating layer.—A covering layer in the electrode center could lead to higher current densities in the uncovered areas, and have similar consequences to the electrode overlap mechanism described above. However, the grey stripe that can be seen in Fig. 8c, which may be a covering layer, only covers about one fifth of its height and fails to extend to the edge area in which the observed inhomogeneities emerge.

Pressure gradients.—The cylindrical cell case can be assumed to have a higher stiffness at the top and bottom than in the center. Upon intercalation-driven expansion of the electrodes during cycling, pressure on the electrodes would be higher in the edge regions compared to the center. This higher pressure could increase current density and electrode utilization and, again, have similar consequences to the electrode overlap mechanism.

In summary, while we may reasonably assume that non-uniform charge distribution causes the loss of accessible capacity, we cannot yet determine the reasons for the non-uniformity with certainty. As a starting point, cylindrical cells with other chemistries than LFP/C

must be investigated in shallow-cycle scenarios. Additionally, temperature and pressure gradients could be applied from the outside to the LFP/C cells used in this study. Furthermore, LFP/C cells in pouch format could provide valuable insights regarding the influence of cell design, especially if their surface temperature could be controlled locally. Finally, the possibility of charge accumulation at electrode edges under some of the proposed scenarios could also be examined using physicochemical models.

Conclusions

This work shows that strongly non-uniform charge distribution may be the cause of significant reversible capacity losses in LFP/C cells. Commercial cylindrical LFP/C cells were cycled continuously with low cycle depths, an experiment which reproduces the operating conditions in primary control reserve applications.[40] Cycling with these low cycle depths led to significantly higher capacity losses than with full cycles. A large portion of the capacity losses with low cycle depths could be recuperated. The most effective recuperation method was holding the cells at their lower cut-off voltage. After recuperation, the relative capacity of low cycle depth cells was higher than that of full cycle cells. DVA, color differences in the graphite anode and experiments with harvested electrode material have provided both direct and indirect experimental evidence of non-uniform charge distribution in the low cycle depth cells.

We have argued that the low potential gradients of LFP and graphite over a large SOC range may not provide enough driving force to re-homogenize the charge distribution in the electrodes, once it has become non-uniform. We have discussed hypotheses based on temperature, entropy and cell design that provide clues for identifying the true origin of the non-uniformity in the future.

ORCID

Franz B. Spingler https://orcid.org/0000-0002-6523-3986
Maik Naumann https://orcid.org/0000-0002-1995-3069
Andreas Jossen https://orcid.org/0000-0003-0964-1405

References

1. J. Wilhelm, S. Seidlmayer, P. Keil, J. Schuster, A. Kriele, R. Gilles, and A. Jossen, *J. Power Sources*, **365**, 327 (2017).
2. M. Lewerenz, J. Münnix, J. Schmalstieg, S. Käbitz, M. Knips, and D. U. Sauer, *J. Power Sources*, **345**, 254 (2017).
3. M. Lewerenz, G. Fuchs, L. Becker, and D. U. Sauer, *Journal of Energy Storage*, **18**, 149 (2018).
4. M. Lewerenz, P. Dechent, and D. U. Sauer, *Journal of Energy Storage*, **21**, 680 (2019).
5. M. Naumann, M. Schimpe, P. Keil, H. C. Hesse, and A. Jossen, *Journal of Energy Storage*, **17**, 153 (2018).
6. M. Naumann, F. B. Spingler, and A. Jossen, *J. Power. Sources.*, **451**, 227 (2020).
7. K. Rumpf, M. Naumann, and A. Jossen, *Journal of Energy Storage*, **14**, 224 (2017).
8. E. Sarasketa-Zabala, I. Gandiaga, E. Martinez-Laserna, L. M. Rodriguez-Martinez, and I. Villarreal, *J. Power Sources*, **275**, 573 (2015).
9. P. Keil and A. Jossen, *Journal of Energy Storage*, **6**, 125 (2016).
10. M. Petzl and M. A. Danzer, *J. Power Sources*, **254**, 80 (2014).
11. C. von Lüders, V. Zinth, S. V. Erhard, P. J. Osswald, M. Hofmann, R. Gilles, and A. Jossen, *J. Power Sources*, **342**, 17 (2017).
12. S. Schindler, M. Bauer, M. Petzl, and M. A. Danzer, *J. Power Sources*, **304**, 170 (2016).
13. I. D. Campbell, M. Marzook, M. Marinescu, and G. J. Offer, *J. Electrochem. Soc.*, **166**, A725 (2019).
14. M. C. Smart, B. V. Ratnakumar, M. C. Smart, and B. V. Ratnakumar, *J. Electrochem. Soc.*, **158**, A379 (2011).
15. M. C. Smart, B. V. Ratnakumar, L. Wbitcanack, K. Chin, M. Rodriguez, and S. Surampudi, *Seventeenth Annual Battery Conference on Applications and Advances* (2002).
16. J. Dahn, *Phys. Rev. B*, **44**, 9170 (1991).
17. T. Ohzuku, *J. Electrochem. Soc.*, **140**, 2490 (1993).
18. M. Dubarry and B. Y. Liaw, *J. Power Sources*, **194**, 541 (2009).
19. S. Schindler and M. A. Danzer, *J. Power Sources*, **343**, 226 (2017).
20. M. Lewerenz, A. Marongiu, A. Warnecke, and D. U. Sauer, *J. Power Sources*, **368**, 57 (2017).
21. D. Guerard and A. Herold, *Carbon*, **13**, 337 (1975).
22. V. A. Nalimova, D. Guérard, M. Lelaurain, and V. Fateev, *Carbon*, **33**, 177 (1995).
23. S. J. Harris, A. Timmons, D. R. Baker, and C. Monroe, *Chem. Phys. Lett.*, **485**, 265 (2010).
24. M. Petzl, M. Kasper, and M. A. Danzer, *J. Power Sources*, **275**, 799 (2015).
25. D. Burow, K. Sergeeva, S. Calles, K. Schorb, A. Börger, C. Roth, and P. Heitjans, *J. Power Sources*, **307**, 806 (2016).
26. Q. Q. Liu, D. J. Xiong, R. Petibon, C. Y. Du, and J. R. Dahn, *J. Electrochem. Soc.*, **163**, A3010 (2016).
27. J. Wandt, P. Jakes, J. Granwehr, R.-A. Eichel, and H. A. Gasteiger, *Mater. Today*, **21**, 231 (2017).
28. Y. Zhao, Y. Patel, T. Zhang, and G. J. Offer, *J. Electrochem. Soc.*, **165**, A3169 (2018).
29. M. Klett, R. Eriksson, J. Groot, P. Svens, K. Ciosek Högström, R. W. Lindström, H. Berg, T. Gustafson, G. Lindbergh, and K. Edström, *J. Power Sources*, **257**, 126 (2014).
30. T. C. Bach, S. F. Schuster, E. Fleder, J. Müller, M. J. Brand, H. Lorrmann, A. Jossen, and G. Sextl, *Journal of Energy Storage*, **5**, 212 (2016).
31. P. J. Osswald, S. V. Erhard, A. Noel, P. Keil, F. M. Kindermann, H. Hoster, and A. Jossen, *J. Power Sources*, **314**, 93 (2016).
32. P. J. Osswald, S. V. Erhard, J. Wilhelm, H. E. Hoster, and A. Jossen, *J. Electrochem. Soc.*, **162**, A2099 (2015).
33. J. Cannarella and C. B. Arnold, *J. Electrochem. Soc.*, **162**, A1365 (2015).
34. M. Tang, P. Albertus, and J. Newman, *J. Electrochem. Soc.*, **156**, A390 (2009).
35. V. V. Viswanathan, D. Choi, D. Wang, W. Xu, S. Towne, R. E. Williford, J.-G. Zhang, J. Liu, and Z. Yang, *J. Power Sources*, **195**, 3720 (2010).
36. Y. Reynier, R. Yazami, and B. Fultz, *J. Power Sources*, **119–121**, 850 (2003).
37. S. J. Bazinski and X. Wang, *J. Electrochem. Soc.*, **161**, A168 (2014).
38. S. J. Drake, D. A. Wetz, J. K. Ostanek, S. P. Miller, J. M. Heinzel, and A. Jain, *J. Power Sources*, **252**, 298 (2014).
39. Y. Zhu and C. Wang, *J. Power Sources*, **196**, 1442 (2011).
40. A. Zeh, M. Müller, M. Naumann, H. Hesse, A. Jossen, and R. Witzmann, *Batteries*, **2**, 29 (2016).